

# Band Offsets at Semiconductor-Oxide Interfaces from Hybrid Density Functional Calculations

Audrius Alkauskas, Peter Broqvist, Fabien Devynck, and Alfredo Pasquarello

*Institute of Theoretical Physics, Ecole Polytechnique Fédérale de Lausanne (EPFL), CH-1015 Lausanne, Switzerland and  
Institut Romand de Recherche Numérique en Physique des Matériaux (IRRMA), CH-1015 Lausanne, Switzerland*

(Dated: May 28, 2018)

Band offsets at semiconductor-oxide interfaces are determined through a scheme based on hybrid density functionals, which incorporate a fraction  $\alpha$  of Hartree-Fock exchange. For each bulk component, the fraction  $\alpha$  is tuned to reproduce the experimental band gap, and the conduction and valence band edges are then located with respect to a reference level. The lineup of the bulk reference levels is determined through an interface calculation, and shown to be almost independent of the fraction  $\alpha$ . Application of this scheme to the Si-SiO<sub>2</sub>, SiC-SiO<sub>2</sub>, and Si-HfO<sub>2</sub> interfaces yields excellent agreement with experiment.

PACS numbers: 71.15.Mb, 73.20.At, 73.40.Qv

The discontinuity in the local band structure at semiconductor-semiconductor and semiconductor-oxide interfaces is a crucial physical property for the operation of most electronic and optoelectronic devices [1]. Early theoretical research [2], mainly on semiconductor heterojunctions, provided a deep understanding of the processes that govern the band alignments at interfaces [3, 4, 5, 6]. This resulted in the development of theoretical models providing a reasonable description of band offsets and being particularly useful when a wide class of materials needs to be screened [7]. However, these models mainly rely on bulk properties of the interface components [2], and therefore do not account for the detailed atomic and electronic properties at the interface, which are known to affect band offsets [8].

Density functional calculations of band offsets provide a qualitative improvement by describing the electronic and atomic arrangements at the interface in a self-consistent way [9, 10, 11, 12, 13]. However, the most common approximations to the exchange-correlation energy, i.e. the generalized-gradient approximation and the local density approximation, lead to significant underestimations of band gaps, thereby impairing the reliability of calculated band offsets. While valence band offsets at semiconductor heterojunctions are described with reasonable accuracy due to cancellation of errors in both interface components, band-offsets errors for semiconductor-oxide interfaces can reach several eV [8, 14, 15, 16]. Calculations based on the *GW* perturbation theory yield accurate band offsets at interfaces due to an improved description of bulk band gaps [17, 18]. However, these calculations are computationally demanding and can only be applied to relatively small systems. For instance, the study of realistic semiconductor-oxide interfaces in which the oxide is noncrystalline [14, 15, 19] is severely hindered.

In this work, we introduce a scheme for calculating band offsets at interfaces through the use of hybrid density functionals. These functionals incorporate a fraction

$\alpha$  of Hartree-Fock exchange [20] and substantially improve the description of bulk band gaps [21]. We apply our scheme to model structures of the Si-SiO<sub>2</sub>, Si-HfO<sub>2</sub>, and SiC-SiO<sub>2</sub> interfaces, which all feature a realistic description of the complex transition region. The band structures of the two interface components are lined up through their reference levels at the interface [11]. For each component, we perform bulk calculations tuning the fraction  $\alpha$  to reproduce the experimental band gap. The lineup of the reference potential in the interface model is found to only weakly depend on the fraction  $\alpha$  conferring consistency on our scheme. For the three interfaces studied, the calculated band offsets are in excellent agreement with experiment.

We considered a class of hybrid density functionals based on the generalized gradient approximation of Perdew, Burke, and Ernzerhof (PBE) [22], which are obtained by replacing a fraction  $\alpha$  of PBE exchange with Hartree-Fock exchange [23]. The functional defined by  $\alpha=0.25$  is referred to as PBE0 and is supported by theoretical considerations [23]. Core-valence interactions were described through normconserving pseudopotentials generated at the PBE level. The valence wave functions were expanded in a plane-wave basis set defined by an energy cutoff of 70 Ry. The interface calculations corresponding to large supercells were performed with a Brillouin-zone sampling restricted to the  $\Gamma$  point. In the bulk calculations, the positions of the band extrema were determined through converged  $k$ -point samplings. The integrable divergence of the Hartree-Fock exchange term was explicitly treated [24]. Structural relaxations were carried out at the PBE level. We used the implementations in QUANTUM-ESPRESSO [25] and CPMD [26].

The choice of the model structures requires particular attention. Indeed, previous density-functional studies on crystalline-crystalline Si-ZrO<sub>2</sub> and SiO<sub>2</sub>-HfO<sub>2</sub> interfaces have revealed a strong sensitivity of the band offsets on the adopted model of the interfacial bonding pattern [8]. Therefore, we considered model interfaces in which the

TABLE I: Band gaps (in eV) of Si, SiC, HfO<sub>2</sub>, and SiO<sub>2</sub>, calculated using functionals incorporating a varying fraction  $\alpha$  of Hartree-Fock exchange:  $\alpha=0$  (PBE),  $\alpha=0.25$  (PBE0), and an optimal fraction  $\alpha_0$  reproducing the experimental band gap.

	PBE	PBE0	Optimal ( $\alpha_0$ )	Expt.
Si	0.6	1.8	1.1 (0.11)	1.1
SiC	2.2	3.9	3.3 (0.15)	3.3
HfO <sub>2</sub>	4.3	6.7	5.9 (0.15)	5.9
SiO <sub>2</sub>	5.4	7.9	8.9 (0.34)	8.9

oxide is amorphous to ensure that the transition region is smooth in terms of bond parameters and coordination [14, 15, 19]. For the Si-SiO<sub>2</sub> interface, such a choice led to variations of 0.1 to 0.2 eV in the band offsets calculated at the PBE level [27]. The Si-SiO<sub>2</sub> interface adopted here is described through a 217-atom superlattice model in which layers of crystalline Si (9 monolayers) and of amorphous SiO<sub>2</sub> (17 Å) alternate [14]. This interface model structure incorporates a set of atomic-scale features inferred from experimental data. The SiC-SiO<sub>2</sub> interface is modeled by a 237-atom slab characterized by a chemically abrupt transition between crystalline 4*H*-SiC (8 monolayers) and amorphous SiO<sub>2</sub> (16 Å) [15]. The Si-HfO<sub>2</sub> interface is described by a superlattice model comprising 282 atoms and including a SiO<sub>2</sub> interlayer (7 Å) between crystalline silicon (10 monolayers) and amorphous HfO<sub>2</sub> (12 Å) [19]. To represent the bulk of the interface components, we used the corresponding crystalline structures for Si and 4*H*-SiC, a disordered model for SiO<sub>2</sub> [28], and the monoclinic structure for HfO<sub>2</sub> [29]. In Table I, the band gaps of these reference bulk components are calculated at the PBE and PBE0 levels and compared to experimental values. As well known, the PBE band gaps severely underestimate their measured counterparts. While the inclusion of Hartree-Fock exchange always enhances the calculated band gap, the comparison with experiment is not systematically improved at the PBE0 level.

First, we calculated band offsets at the three interfaces within both PBE and PBE0. The bulk band edges were aligned through a reference potential calculated across the interface [11]. As reference potential, we generally used the local potential [30], but for SiO<sub>2</sub> and HfO<sub>2</sub> we resorted to the energy levels of the deep O 2*s* and Hf 5*s* states which are less sensitive to structural disorder. Focusing on the Si-SiO<sub>2</sub> interface, we show in Fig. 1 the planar-averaged electron density and local potential across the interface. With respect to PBE, PBE0 only yields a small redistribution of the electron density [Fig. 1(b)], which results in a difference of  $\Delta V=0.16$  eV between the lineups of the potentials at the interface [Fig. 1(d)]. This indicates that the dipole contribution to the band offsets is already well described at the PBE level.

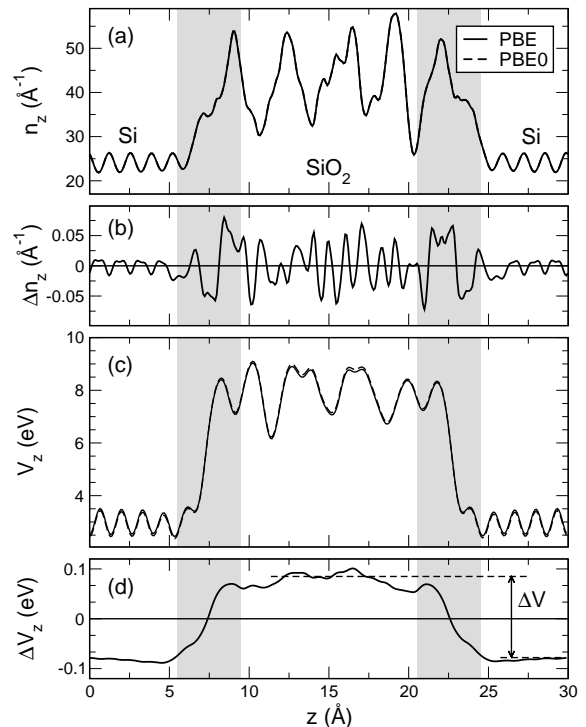


FIG. 1: Planar-averaged (a) electron density and (c) local potential across the Si-SiO<sub>2</sub> interface calculated in PBE (solid) and PBE0 (dashed). The difference between the electron densities and the local potentials in the two schemes is shown in (b) and (d), respectively. The shaded areas correspond to the transition regions between Si and SiO<sub>2</sub>.

TABLE II: Valence ( $\Delta E_v$ ) and conduction ( $\Delta E_c$ ) band offsets at the Si-SiO<sub>2</sub>, SiC-SiO<sub>2</sub>, and Si-HfO<sub>2</sub> interfaces calculated in PBE, PBE0, and the mixed scheme. Experimental band offsets are from Refs. [31], [34], and [35], respectively.

		PBE	PBE0	Mixed	Expt.
Si/SiO <sub>2</sub>	$\Delta E_v$	2.5	3.3	4.4	4.4
	$\Delta E_c$	2.3	2.7	3.4	3.4
4 <i>H</i> -SiC/SiO <sub>2</sub>	$\Delta E_v$	1.4	2.0	3.0	2.9
	$\Delta E_c$	1.7	2.0	2.6	2.7
Si/HfO <sub>2</sub>	$\Delta E_v$	2.3	3.1	2.9	2.9
	$\Delta E_c$	1.5	1.9	1.7	1.7

Nevertheless, band offsets calculated at the PBE0 level noticeably improve upon the PBE ones. For instance the valence band offset goes from 2.5 eV to 3.3 eV, to be compared with the experimental value of 4.4 eV [31]. This improvement is mostly due to a better description of bulk band gaps in PBE0 (Table I). However, deviations with respect to experiment are still remarkable. Similar observations also hold for the other interfaces (Table II).

To further improve band offsets, it appears imperative to more accurately describe the band gaps of bulk components. This cannot be achieved for both interface components through the use of a hybrid functional with

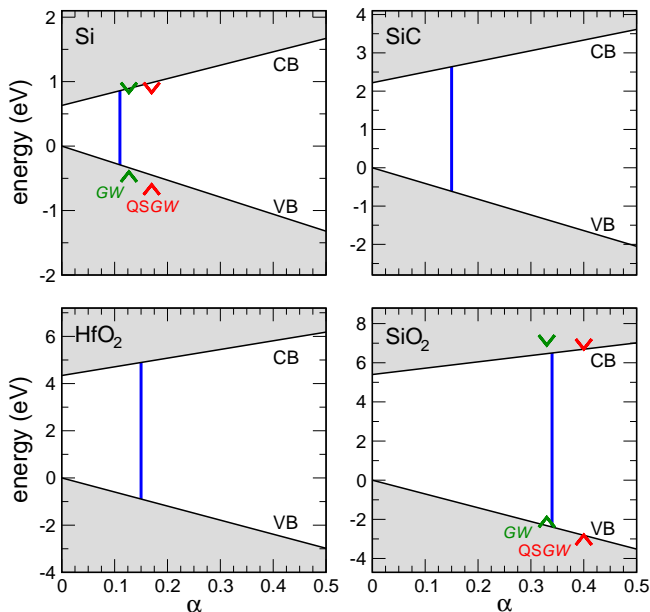


FIG. 2: (color online) Valence band maximum and conduction band minimum vs  $\alpha$  for four different materials. Shifts calculated with *GW* and quasiparticle self-consistent *GW* (QSGW) [18] are also shown. Vertical lines represent the experimental band gaps and are shown in correspondence of  $\alpha_0$  (see text).

a fixed fraction of Hartree-Fock exchange  $\alpha$ . However, it has been argued that there is no universal fraction  $\alpha$  for all materials and that its optimal value could even be property dependent [32]. In Fig. 2, we show the evolution of the conduction and valence band edges of the four bulk materials considered in this work as a function of  $\alpha$ . Since the bulk band gaps increase linearly with  $\alpha$ , the value of  $\alpha$  can always be chosen to reproduce the experimental band gap. This resulted in optimal values  $\alpha_0$  of 0.11 for Si, 0.15 for SiC and HfO<sub>2</sub>, and 0.34 for SiO<sub>2</sub> (Table I and Fig. 2). We note that for these  $\alpha_0$  values, the hybrid functional calculation not only gives the experimental band gap but also the position of the band extrema with respect to the adopted reference potential.

The consideration of a fraction  $\alpha$  of the Hartree-Fock exchange is equivalent to an effective static screening of the long-range interaction:  $\alpha \sim 1/\epsilon_\infty$ , where  $\epsilon_\infty$  is the electronic part of the dielectric constant. Indeed, the optimal  $\alpha_0$ 's found above respect this relationship in a qualitative way. To further support the proposed adjustment of  $\alpha$ , we compared the band shifts of Si and SiO<sub>2</sub> calculated with the hybrid functionals to those obtained with *GW* and quasiparticle selfconsistent *GW* (QSGW) [18]. The *GW* band shifts are reported in Fig. 2 in correspondence of the value of  $\alpha$  which reproduces the band gap found in the *GW* calculation. The comparison between hybrid and *GW* band shifts is quite good, with differences not exceeding those between different *GW* schemes.

The observations above can be combined to obtain

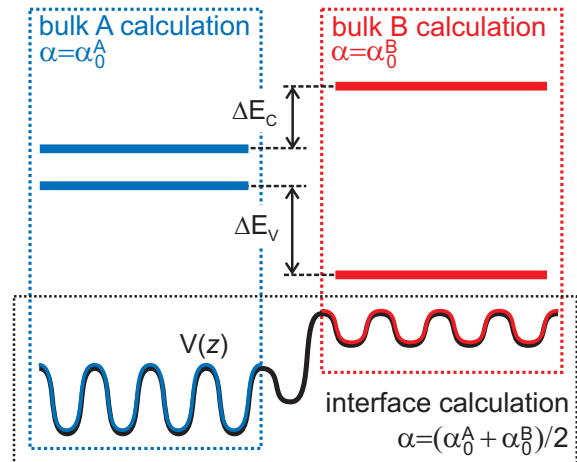


FIG. 3: (Color online) Schematic illustration of band offset determination at the interface between components *A* and *B* through the mixed scheme (see text). The local potential  $V(z)$  is obtained from an interface calculation based on a hybrid functional with  $\alpha = (\alpha_0^A + \alpha_0^B)/2$  and determines the lineup of the reference levels in the two components. For each component, the band extrema are then aligned to the reference potential through bulk calculations based on hybrid functionals with a material-specific  $\alpha_0$  chosen to reproduce its experimental band gap.  $\Delta E_v$  and  $\Delta E_c$  are the resulting valence and conduction band offsets.

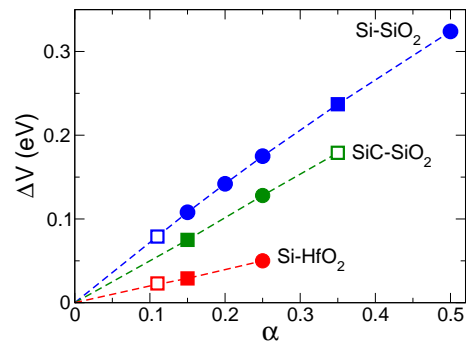


FIG. 4: (Color online) Lineup of the local potential (filled circles), expressed as a difference with respect to the result obtained with PBE ( $\alpha=0$ ), vs fraction of Hartree-Fock for the Si-SiO<sub>2</sub>, SiC-SiO<sub>2</sub>, and Si-HfO<sub>2</sub> interfaces. Squares are shown in correspondence of the  $\alpha_0$ 's of the individual bulk components (0.11 for Si, 0.15 for SiC and HfO<sub>2</sub>, and 0.34 for SiO<sub>2</sub>). Filled symbols correspond to actual calculations, while open symbols are positioned by interpolation or extrapolation.

band offsets. From the interface model, the lineup of the reference potentials in the two bulk components is determined. Then, bulk extrema are positioned on each side of the interface using the results of hybrid functional calculations with optimal  $\alpha_0$  for each bulk component [33]. This mixed scheme is graphically illustrated in Fig. 3.

The scheme critically relies on the fact that the lineup extracted from the interface calculation is not significantly dependent on the adopted fraction of Hartree-Fock

exchange  $\alpha$ . To further support this point, we performed several hybrid functional calculations with varying  $\alpha$  for each of the model interfaces under consideration. As shown in Fig. 4, the lineup between the reference levels in the two bulk components only marginally depends on  $\alpha$ , generalizing the observation made above for the Si-SiO<sub>2</sub> interface. The dependence on  $\alpha$  is even weaker for the other interfaces. Inspection of Fig. 1(b) shows that the charge transfer occurring at the interface is similar to that observed in the oxide, suggesting that the change of the interfacial dipole should be attributed to a modification of the local chemistry rather than to the increase of the number semiconductor-induced gap states [6] resulting from the modified band offsets. Assuming that the interface calculation is performed with a value of  $\alpha$  corresponding to the average of the  $\alpha_0$ 's pertaining to the two interface components, we estimate that the induced indetermination is smaller than 0.15 eV in the worst case.

The band offsets obtained through the application of the mixed scheme are included in Table II. The calculated values agree extremely well with experimental ones. The error between theory and experiment is similar to the intrinsic indetermination of our approach and to the scatter between different experiments. In comparison to hybrid calculations with a fixed fraction  $\alpha$ , the mixed scheme provides a striking improvement in the theoretical estimation of band offsets.

In conclusion, we demonstrated the accurate determination of band offsets through the use of hybrid density functionals and experimental band gaps. The presented scheme constitutes a predictive tool which is computationally less demanding than *GW* calculations, yet achieves band offsets of comparable accuracy [18]. Its application to complex interface components such as non-crystalline oxides is within reach without loss of accuracy.

Support from the Swiss National Science Foundation (Grants Nos. 200020-111747 and 200020-119733) is acknowledged. The calculations were performed on the BlueGene of EPFL, at DIT-EPFL and CSCS.

---

[1] S. M. Sze, *Physics of Semiconductor Devices* (John Wiley & Sons, New York, 1981).  
 [2] For a review, see J. Tersoff, in *Heterojunction Band Discontinuities: Physics and Device Application*, edited by F. Capasso and G. Margaritondo (North-Holland, Amsterdam, 1987).  
 [3] W. R. Frensley and H. Kroemer, Phys. Rev. B **16**, 2642 (1977).  
 [4] W. A. Harrison, J. Vac. Sci. Technol **14**, 1016 (1977).  
 [5] C. Tejedor and F. Flores, J. Phys. C: Solid State Phys. **11**, L19 (1978).  
 [6] J. Tersoff, Phys. Rev. B **30**, 4874 (1984).  
 [7] J. Robertson, J. Vac. Sci. Technol. B **18**, 1785 (2000).

[8] P. W. Peacock and J. Robertson, Phys. Rev. Lett. **92**, 057601 (2004); O. Sharia *et al.*, Phys. Rev. B **75**, 035306 (2007).  
 [9] G. A. Baraff, J. A. Appelbaum, and D. R. Hamann, Phys. Rev. Lett. **38**, 237 (1977).  
 [10] W. E. Pickett, S. G. Louie, and M. L. Cohen, Phys. Rev. B **17**, 815 (1978).  
 [11] C. G. Van de Walle and R. M. Martin, Phys. Rev. B **35**, 8154 (1987).  
 [12] S.-H. Wei and A. Zunger, Appl. Phys. Lett. **72**, 2011 (1998).  
 [13] N. Peressi, N. Binggeli, and A. Baldereschi, J. Phys. D: Appl. Phys. **31**, 1273 (1998).  
 [14] F. Giustino and A. Pasquarello, Phys. Rev. Lett. **95**, 187402 (2005); A. Bongiorno *et al.*, Phys. Rev. Lett. **90**, 186101 (2003); A. Bongiorno and A. Pasquarello, Appl. Phys. Lett. **83**, 1417 (2003).  
 [15] F. Devynck *et al.*, Phys. Rev. B **76**, 075351 (2007).  
 [16] J. Godet, P. Broqvist, and A. Pasquarello, Appl. Phys. Lett. **91**, 262901 (2007).  
 [17] S. B. Zhang *et al.*, Solid State Commun. **66**, 585 (1988).  
 [18] R. Shaltaf *et al.*, Phys. Rev. Lett. **100**, 186401 (2008).  
 [19] P. Broqvist, A. Alkauskas, and A. Pasquarello, Appl. Phys. Lett. **92**, 132911 (2008).  
 [20] A. D. Becke, J. Chem. Phys. **98**, 5648 (1993).  
 [21] J. Muscat, A. Wander, and N. M. Harrison, Chem. Phys. Lett. **342**, 397 (2001); J. Paier *et al.*, J. Chem. Phys. **124**, 154709 (2006).  
 [22] J. P. Perdew, K. Burke, and M. Ernzerhof, Phys. Rev. Lett. **77**, 3865 (1996).  
 [23] J. P. Perdew, M. Ernzerhof, and K. Burke, J. Chem. Phys. **105**, 9982 (1996).  
 [24] F. Gygi and A. Baldereschi, Phys. Rev. B **34**, 4405 (1986).  
 [25] <http://www.quantum-espresso.org>.  
 [26] R. Car and M. Parrinello, Phys. Rev. Lett. **55**, 2471 (1985); J. Hutter and A. Curioni, ChemPhysChem **6**, 1788 (2005); CPMD, Copyright IBM Corp 1990-2006, Copyright MPI für Festkörperforschung Stuttgart 1997-2001.  
 [27] F. Giustino, A. Bongiorno, and A. Pasquarello, Appl. Phys. Lett. **86**, 192901 (2005); F. Giustino and A. Pasquarello, Surf. Sci. **586**, 183 (2005).  
 [28] J. Sarnthein, A. Pasquarello, and R. Car, Phys. Rev. Lett. **74**, 4682 (1995); Phys. Rev. B **52**, 12690 (1995).  
 [29] P. Broqvist and A. Pasquarello, Appl. Phys. Lett. **89**, 262904 (2006).  
 [30] The local potential comprises the local part of the pseudopotential and the electrostatic potential.  
 [31] F.J. Himpsel *et al.*, Phys. Rev. B **38**, 6084 (1988); J. W. Keister *et al.*, J. Vac. Sci. Technol. B **17**, 1831 (1999).  
 [32] M. Ernzerhof, J. P. Perdew, and K. Burke, Int. J. Quantum Chem. **64**, 285 (1997); M. Ernzerhof and G. Scuseria, J. Chem. Phys. **110**, 5029 (1999).  
 [33] When a Kohn-Sham level is used as reference potential, the bulk calculation is first performed with the same  $\alpha$  as in the interface calculation. The band edges are then adjusted according to Fig. 2.  
 [34] V. V. Afanas'ev *et al.*, J. Phys.: Condens. Matter **14**, S1839 (2004).  
 [35] M. Oshima *et al.*, Appl. Phys. Lett. **83**, 2172 (2003); O. Renault *et al.*, Surf. Sci. **566-568**, 526 (2004).